Journal of Hazardous Materials, 33 (1993) 75–99
Elsevier Science Publishers B.V., Amsterdam

Forced, angled plumes

G.F. Lane-Serff[a], P.F. Linden[b] and M. Hillel[b]

[a] *Department of Oceanography, Highfield, Southampton SO9 5NH (UK)*
[b] *Department of Applied Mathematics and Theoretical Physics, Silver Street, Cambridge CB3 9EW (UK)*

(Received November 15, 1991; accepted in revised form July 3, 1992)

Abstract

In this paper a simple mathematical model is used to describe the curved, turbulent plume formed by injecting a constant flux of buoyant fluid into a stationary, unstratified ambient at an angle to the vertical. The main assumptions are the entrainment assumption: the entrainment into the turbulent plume is at a rate proportional to the local mean along-plume velocity, and the Boussinesq approximation: the density difference between the plume and the ambient is relatively small. A unified theory is presented which allows practical predictions to be made of plume trajectories and concentrations without recourse to complex turbulent modelling. It is found that *all* such plumes can be traced back to a virtual origin, and that the *shape* of the plume depends only on the angle of the plume to the vertical at the virtual origin. Various properties of the plume such as mean velocity, radius and density are predicted as functions of distance along the plume. Angled plumes made in laboratory experiments are described and compared with the theoretical predictions. The applications and limitations of the theoretical model are discussed.

1. Introduction

Forced, angled plumes occur in a variety of situations, wherever relatively dense or light fluid is injected at an angle into a large body of fluid. Thus this flow occurs both naturally and due to the action of man; for example in magma chambers, flows into lakes and seas (especially where the outflow is below the surface), sewage outfalls, ventilation systems, accidental leaks of gases and other hazardous materials and vehicle exhausts. In such flows the plume of relatively light (or dense) fluid will be turbulent and ambient fluid will be mixed into the plume by turbulent eddies. This paper describes a simple theoretical model of these forced, angled plumes which shows how all such plumes can be traced back to a virtual origin. Furthermore, the model shows that the shape of the plume depends only on the angle of the plume to the vertical at the virtual origin.

Correspondence to: Dr. P.F. Linden, Department of Applied Mathematics and Theoretical Physics, Silver Street, Cambridge CB3 9EW (UK).

The nature of plumes rising from sources of buoyancy and momentum has been discussed and described by many authors. Morton et al. [1] set out an analysis of a source of buoyancy, and Morton [2, 3] extended this to allow for a source of buoyancy, mass and momentum. Morton only considered the case where momentum is in the vertical direction and of the same sign as the buoyancy forces: the so called "forced plume". Germeles [4] considered the case of momentum at an angle to the vertical but his analysis breaks down for horizontal plumes. Numerical schemes for evaluating forced, angled plumes from a given set of initial conditions have been described by Schatzmann [5] and Hofer and Hutter [6]. This paper sets out a more general, though simple, analysis of maintained, forced, angled plumes in an unstratified and stationary ambient fluid, with the results given in a form of practical use.

In order to describe this process a simple "entrainment assumption" is made, first proposed by Taylor [7]. The analysis in this paper is based on this assumption and the development of it by Morton et al. [1] and Morton [2, 3]. If the flow is fully turbulent (i.e. independent of Reynolds number) then the flow of ambient fluid into the plume may be described in terms of the relative velocity of the plume to the ambient fluid. The entrainment assumption states that the rate of transfer of ambient fluid into the plume, characterised by an inflow speed of ambient fluid perpendicular to the plume axis, is *proportional* to the mean centre-line speed of the plume (see Fig. 1). The (constant) ratio of inflow speed to plume speed will be denoted by α.

It is known that, for a vertical plume, properties such as time-averaged velocity and density difference follow a Gaussian distribution across the plume (see List [8], for a review), but it is adequate to assume a "top-hat" profile for such quantities, i.e. a uniform value across the plume and zero outside the plume. In fact, provided it is assumed that the profiles are similar at all positions along the plume, the analysis is not substantially altered by this assumption [2, 3]. The length-scale over which the density difference profile spreads is known to be larger than that over which the velocity profile spreads. We will use λ to denote the ratio of transverse length scales of density and velocity, and take it to be 1.1 based on the results of the experiments mentioned above.

In vertical plumes in unstratified surroundings the entrainment assumption is equivalent to assuming that the plumes are self-similar [9]. We will take $\alpha = 0.1$ from the results obtained by many experimenters [10–12]. The nature of the entrainment, and thus the value of α, may vary between different parts of the flow depending on the relative importance of buoyancy and momentum, but we will ignore such variations since the dominant effect in this problem is the change in entrainment due to the variations in the plume speed at different points on the plume. Thus we are using a somewhat approximate, representative value of α. We will discuss variations in α in more detail in the concluding section. We will also assume that fluxes due to variations from the mean flow ("turbulent transports") are insignificant compared with the mean fluxes.

We will assume, further, that the density difference between the plume and the ambient fluid is relatively small (the Boussinesq approximation) and that

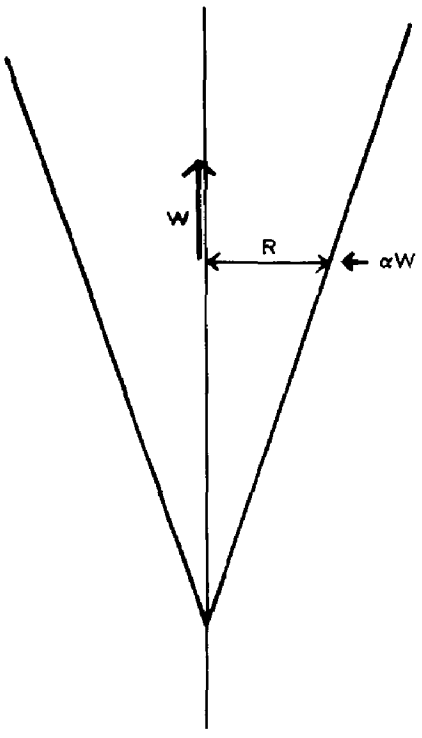

Fig. 1. Idealised view of a vertical plume, with mean centre-line speed W and radius R. The plume entrains ambient fluid characterised by a mean entrainment velocity proportional to the centre-line speed.

the fluid is incompressible. The Boussinesq approximation is not a serious restriction in practice since many of the applications involve relatively small density differences. Also the density difference decreases rapidly away from the source, due to entrainment, and so even when this approximation is not valid near the source it will be valid some distance (usually small) from the source.

The case of forced vertical plumes is re-analysed in Section 2. We develop a new classification and show that vertical plumes fall into three classes depending on the direction of the momentum flux at the virtual origin. The model for angled, forced plumes is given in Section 3 and solutions of the equations for a comprehensive range of source conditions is given in Section 4. These solutions are discussed in Section 5. Experiments on laboratory plumes are described and compared with the model in Sections 6 and 7, and the conclusions of the work are given in Section 8.

2. Vertical forced plumes

We begin with the case of vertical forced plumes in uniform surroundings. Although this has been discussed before (see, for example, Ref. [9], chapter 6)

the results will be presented in a new way which clarifies the division of vertical plumes into three basic categories, namely *buoyant jets*, *mass-sources* and *pure plumes*. This analysis also leads more naturally into the case of plumes directed at other angles, which will be discussed in the later sections. Under the assumptions detailed above, and taking top-hat profiles, the equations of conservation of momentum, mass and buoyancy are, respectively,

$$\begin{aligned} &\mathrm{d}(W^2R^2)/\mathrm{d}Z = g'(\lambda R)^2, \\ &\mathrm{d}(WR^2)/\mathrm{d}Z = 2R\alpha W, \\ &\mathrm{d}(g'WR^2)/\mathrm{d}Z = 0. \end{aligned} \tag{1}$$

Here W is the plume speed, R the plume radius, Z the vertical position and $g' = g\Delta\rho/\rho$ is the reduced gravitational acceleration. We will take g' to be positive and Z to increase along the direction of the buoyancy force, so that Z increases upward for buoyant plumes and downward for negatively buoyant plumes.

It is useful to define

$$\begin{aligned} F &= g'WR^2, \\ K &= WR^2, \\ P &= W^2R^2. \end{aligned} \tag{2}$$

The quantities F, K and P are proportional to the fluxes of buoyancy, mass and momentum, respectively. It can be seen immediately from eq. (1) that the buoyancy flux is conserved along the plume and thus

$$F = F_S, \text{ constant}, \tag{3}$$

and F_S is taken here to be positive.

Equations (1) will be non-dimensionalised by the following transformations (using lower-case to denote non-dimensional quantities):

$$\begin{aligned} p &= P/P_S, \\ k &= (\lambda/(2\alpha)^{1/2})F_S^{1/2}P_S^{-5/4}K, \\ z &= ((2\alpha)^{1/2}\lambda)F_S^{1/2}P_S^{-3/4}Z, \\ r &= (z/Z)R, \end{aligned} \tag{4}$$

where F_S and P_S are the values of F and P at the source (the subscript S will refer to conditions at the source throughout this analysis). Substitution of (4) into (1) and (3) leads to

$$\begin{aligned} pp' &= k, \\ k' &= |p|^{1/2}, \end{aligned} \tag{5a}$$

where the primes indicate differentiation with respect to z (except for g'). The initial conditions are

$$p = 1 \quad \text{and} \quad k = k_S = (\lambda/(2\alpha)^{1/2})F_S^{1/2}P_S^{-5/4}K_S. \tag{5b}$$

Integration of (5a) and applying the initial conditions (5b) gives

$$(\tfrac{4}{5})(|p|^{5/2}-1)=k^2-k_S^2. \tag{6}$$

Curves of p against k are plotted in Fig. 2. At the source $p=1$, and from (1a) it can be seen that the momentum flux increases with distance from the source and this is represented on Fig. 2 by the region $p>1$. In the region $p<1$ the solution has been integrated back to a "virtual origin" where the mass flux, k, and hence the plume radius are both zero. The momentum flux, p, is not, in general, zero at the virtual origin and the sign of p at $k=0$ determines the nature of the plume. From (6) it can be seen that the momentum flux at $k=0$ is positive (negative) when the mass flux k_S at the source is less (greater) than the critical value $k_C=2/\sqrt{5}$.

For small values of the mass flux $k_S<k_C$, the momentum and buoyancy fluxes at the virtual origin are in the same direction, and we will refer to this case as the *buoyant jet*. The virtual origin lies behind the source and the initial spread from the source is large. At large distances from the source the solution (for k tending to infinity) asymptotes to that of a pure plume. A sketch of this case is shown in Fig. 3a.

When $k_S=k_C$, the mass and momentum fluxes at the virtual origin are zero and the flow is that of a *pure plume*. In this case the properties of the plume can be derived directly from (5a) with the initial condition $p=0$ at $k=0$. The solution is well known; for the purposes of this analysis it is sufficient to note that the plume is conical with the half-angle at the vertex being $\tan^{-1}(6\alpha/5)$ as shown in Fig. 3b.

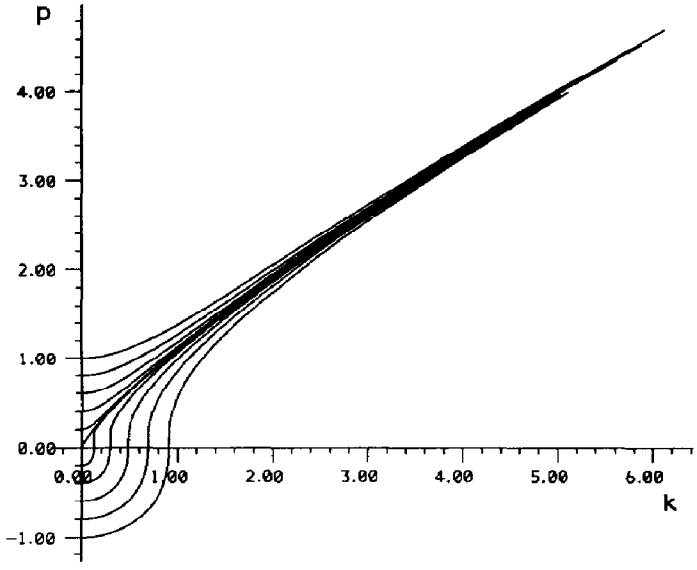

Fig. 2. Momentum and mass fluxes for vertical plumes (non-dimensionalised with respect to the buoyancy and momentum fluxes at the source). The source initial conditions are $p=1$ and $k=k_S$; the solutions have been integrated back to the 'virtual origin' where $k=0$ (and thus the radius equals zero).

For larger values of k_S, so that $k_S > k_C$, $p < 0$ at the virtual origin. In this case the momentum flux at the virtual origin has the opposite sign to the buoyancy flux, and the virtual origin may be in front of the source. At these high values of the source mass flux the plume behaves as though it initially flows backward from the virtual origin, spreading with the same angle as for a jet, its momentum being decelerated by the buoyancy forces until it stops at some point behind the source. It is then accelerated forwards through the source with the required mass and momentum fluxes. This situation is sketched in Fig. 3c and we shall refer to this flow as a *mass source*. It should be emphasised that the

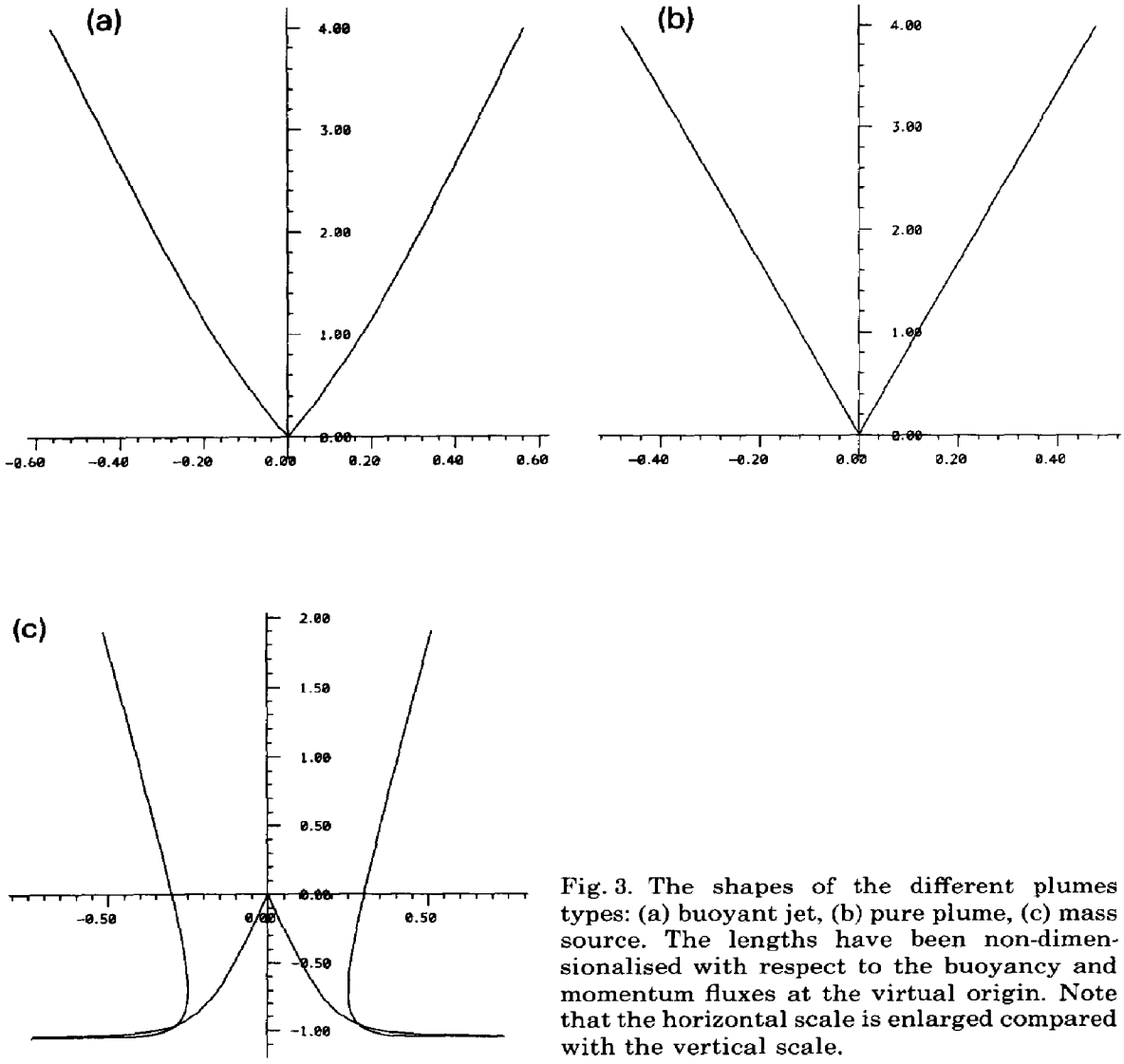

Fig. 3. The shapes of the different plumes types: (a) buoyant jet, (b) pure plume, (c) mass source. The lengths have been non-dimensionalised with respect to the buoyancy and momentum fluxes at the virtual origin. Note that the horizontal scale is enlarged compared with the vertical scale.

region $p<0$ in Fig. 2 is unphysical. We have not considered the case where the momentum and buoyancy fluxes *at the source* have opposite signs. This model does not allow for the plume overlapping itself, nor does it allow for the entrainment of other than ambient fluid. The real source may be anywhere on the upward flowing part of the shape in Fig. 3c, in particular the flow may contract above the source before widening again. Note that the source diameter is never much less than 0.4, in non-dimensional units, and so the plume shape is very close to a buoyant plume only a few diameters from the source. For this reason the mass-source type flow is generally regarded as an unimportant case for vertical plumes, but we include it for completeness and for comparison with downward pointing angled plumes for which the downward flowing part is a physical solution since the plume would then entrain ambient fluid.

It is convenient to non-dimensionalise the equations of motion with respect to the momentum flux at the virtual origin, P_0, rather than that at the source. We will denote this new set of non-dimensional quantities by the subscript 1, i.e.

$$
\begin{aligned}
&p_1 = P/P_0, \\
&k_1 = (\lambda/(2\alpha)^{1/2}) F_S^{1/2} P_0^{-5/4} K, \\
&z_1 = ((2\alpha)^{1/2}\lambda) F_S^{1/2} P_0^{-3/4} Z, \\
&r_1 = (z_1/Z) R, \quad \text{and so } k_{1S} = (\lambda/(2\alpha)^{1/2}) F_S^{1/2} P_0^{-5/4} K_S.
\end{aligned}
\tag{7}
$$

With this non-dimensionalisation the curves in Fig. 2 are reduced to the three curves shown in Fig. 4. Instead of the source conditions being represented by the point where $p=1$ and $k=k_S$ on Fig. 2, they are represented on Fig. 4 by the point where $p_1=p_{1S}=P_S/P_0$ and $k_1=k_{1S}$. This will be on the curve marked "buoyant jet" if $k_S<k_C$: all curves above the pure plume curve are mapped onto the jet-curve. Whereas it will be on the curve marked "mass-source" if $k_S>k_C$: all curves below the pure plume curve are mapped onto the mass-source curve (see Fig. 5). The shape of the plume thus depends only on whether k_S is greater or less than k_C. The size of the plume is determined by the length scale

$$
L_v = (1/(2\alpha)^{1/2}\lambda) F_S^{-1/2} P_0^{3/4}, \tag{8}
$$

where $P_0 = |1-\frac{5}{4}k_S^2|^{2/5} P_S$ (with k_S defined in eq. 5b).

Note that as k_S approaches k_C, from either direction, the length scale tends to zero, and hence the extent of the region where the plume shape differs significantly from that of the pure plume also tends to zero and the non-dimensional distance of the actual source from the virtual origin tends to infinity. In Fig. 6, p_1 and k_1 are plotted against z_1, and thus the position of the actual source in Fig. 3 can be found as the value of z_1 for which $k_1=k_{1S}$. The part of the mass-source curves where z_1 is decreasing as p_1 and k_1 increase is not physical, it represents a downward flowing plume entraining ambient fluid.

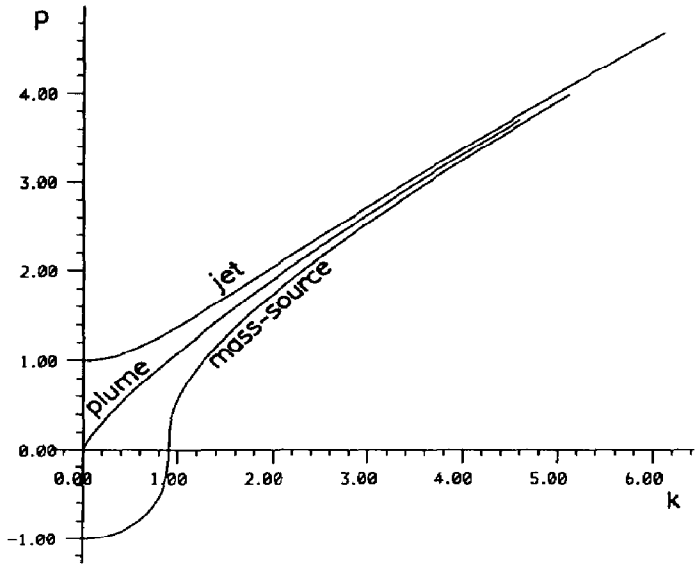

Fig. 4. Momentum and mass fluxes non-dimensionalised with respect to the buoyancy and momentum fluxes at the virtual origin. The family of solutions in Fig. 2 is reduced to just three here.

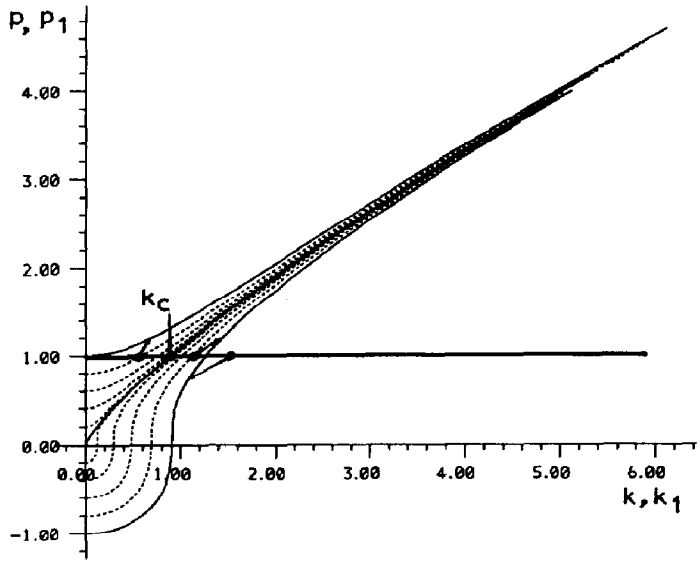

Fig. 5. The non-dimensionalisation from $p=1$, $k=k_S$, to $p_1=p_{1S}$, $k_1=k_{1S}$. All solutions in the 'jet region' are mapped to the buoyant jet curve, whilst those in the 'mass source region' are mapped to the mass source curve.

For the case of a pure plume, the distance Z_V from the source to the virtual origin is related to the source radius, R_S, by

$$R_S=(6\alpha/5)Z_V,$$

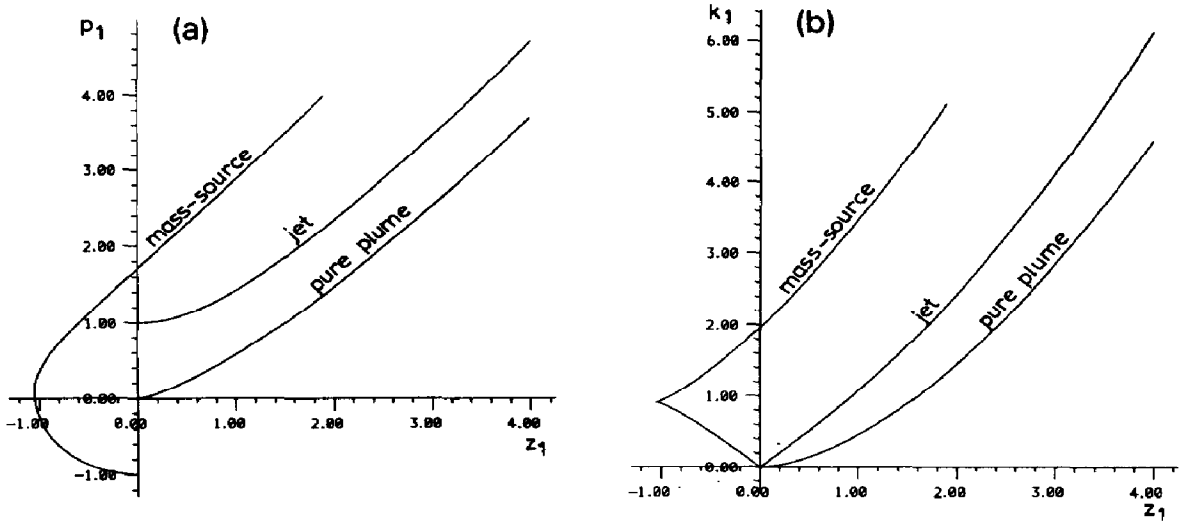

Fig. 6. Momentum and mass fluxes as functions of height for the three plume types. (All quantities non-dimensionalised with respect to the buoyancy and momentum fluxes at the virtual origin.)

since, as mentioned above, the pure plume is straight sided. Consequently R is given by

$$R=(Z+Z_V)R_S/Z_V.$$

Recall that Z is the distance above the actual source, and thus the results familiar from similarity solutions of buoyant axisymmetric plumes are recovered,

$$\begin{aligned} W&=W_S(R_S/R)^{1/3}=W_S(Z_V/(Z+Z_V))^{1/3},\\ \Delta\rho&=\rho g'/g=\Delta\rho_S(R_S/R)^{5/3}=\Delta\rho_S(Z_V/(Z+Z_V))^{5/3}. \end{aligned} \tag{9}$$

For the other plume types such quantities can be calculated from the values of p_1 and k_1 given in Fig. 6,

$$\begin{aligned} \Delta\rho&=\rho g'/g=\Delta\rho_S k_{1S}/k_1,\\ R&=R_S(k_1/k_{1S})(p_{1S}/p_1)^{1/2},\\ W&=W_S(k_{1S}/k_1)(p_1/p_{1S}), \end{aligned} \tag{10}$$

In order to understand the nature of the changing length scales and shapes, consider a source of buoyant fluid with a fixed total flow rate but a variable exit size. This fixes buoyancy and mass fluxes, but if the exit radius is reduced the efflux velocity and thus the momentum flux must increase. Starting with a large exit radius, P_S will be small and k_S will be large. On changing scales to p_1 and k_1 it can be seen that p_{1S} is small and k_{1S} is greater than k_C. The source will have the shape shown in Fig. 3 for a "mass source", with a large length

scale ($L_V = (5^{3/10}/2)(K_S^3/4\lambda^2\alpha^4 F_S)^{1/5}$, from eq. 8) and with the source position close to $z_1 = 0$. In practice the entrainment assumption is likely to be inaccurate near such a source as the plume will not be fully turbulent there. This will result in a more pinched shape than that shown in Fig. 3c.

As the exit radius is reduced so P_S increases. The shape of the plume will remain the same but the length scale L_V will decrease, and so the plume will tend to the straight-sided buoyant plume shape closer to the source. Also z_{1S} will increase, so the actual position of the source will be higher on the mass source shape (Fig. 3c). As the radius is reduced further, k_S approaches k_C, and p_{1S}, k_{1S} and z_{1S} tend to infinity, the length scale L_V tends to zero and the shape will be that of a straight-sided pure plume (Fig. 3b). Reducing the radius still further, k_S becomes less than k_C, and p_{1S}, k_{1S} and z_{1S} are still large and the shape is still close to that of the buoyant plume. Now, however, the plume follows the "buoyant jet" shape (Fig. 3a) with the plume spreading at an angle which decreases with height rather than increases as for the mass source shape (compare Figs. 3a and 3c). As the exit radius is further reduced k_S tends to zero, P_0 tends to P_S, the length scale, L_V, behaves like $P_S^{3/4}$, k_{1S} tends to k_S and z_{1S} tends to zero (to the apex of the jet shape) giving an initial spreading angle of $\tan^{-1}(2\alpha)$.

3. The model for forced, angled plumes

Now consider forced plumes where the initial momentum flux is not purely vertical but is at an angle to the vertical. Again the entrainment assumption is applied by stating that the inflow speed into the plume is proportional to the speed along the centre-line of the plume. Ignoring the curvature of the plume the "top-hat" equations become (for flow in an unstratified medium)

$$\begin{aligned} &\textit{Momentum} \\ &\quad \text{vertical} && \mathrm{d}(WVR^2)/\mathrm{d}S = g'(\lambda R)^2, \\ &\quad \text{horizontal} && \mathrm{d}(UVR^2)/\mathrm{d}S = 0, \\ &\textit{Mass} && \mathrm{d}(VR^2)/\mathrm{d}S = 2R\alpha V, \\ &\textit{Density} && \mathrm{d}(g'VR^2)/\mathrm{d}S = 0. \end{aligned} \tag{11}$$

In this case U and W are the horizontal and vertical components of the centre-line velocity, $V = (U^2 + W^2)^{1/2}$, R is the radius of the plume and S is the distance along the plume centre-line (see Fig. 7). As before $g' = g\Delta\rho/\rho$ is the reduced gravity. The inclination of the plume to the horizontal, θ, is given (for any point on the plume centre-line) by $\tan\theta = W/U$.

It is useful to define

$$F = g'VR^2, \qquad Q = VR^2, \qquad M = V^2R^2, \qquad H = UVR^2, \tag{12}$$

which are proportional to the total buoyancy, mass and momentum fluxes and the horizontal momentum flux, respectively (compare with eq. 2).

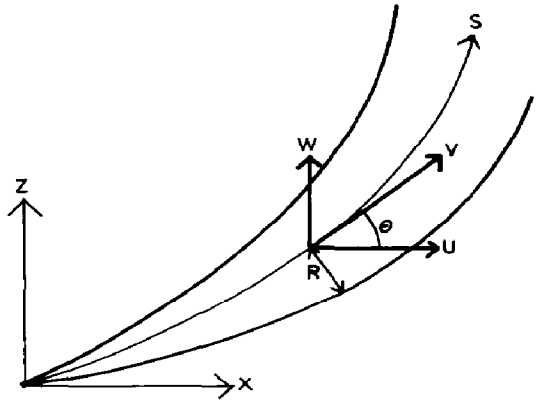

Fig. 7. An idealised view of an angled plume. Compare this with Fig. 1.

From (11) it can immediately be seen that the horizontal momentum flux, H_0, and the buoyancy flux, F_0, are conserved along the plume,

$$F_0 = g' VR^2, \quad \text{constant},$$
$$H_0 = UVR^2, \quad \text{constant}. \tag{13}$$

These conserved quantities are used to define non-dimensional variables (in this case there is no need to integrate back to the virtual origin to find a meaningful scale for the momentum flux, unlike the vertical plume described above)

$$m = M/H_0, \qquad q = (\lambda/(2\alpha)^{1/2}) H_0^{-5/4} F_0^{1/2} Q,$$
$$s = S/L_A, \qquad r = R/L_A, \qquad x = X/L_A, \qquad z = Z/L_A, \tag{14}$$

where the length-scale is given by $L_A = (\lambda\sqrt{\alpha})^{-1} H_0^{3/4} F_0^{-1/2}$. The remaining plume equations (11) then reduce to the pair of equations

$$m((m^2-1)^{1/2})' = q,$$
$$q' = (m)^{1/2}, \tag{15}$$

where the primes now represent differentiation with respect to s, i.e. along the plume axis (except again for g').

This form of the equations breaks down as θ tends to $\pm\pi/2$. In this limit, $m \gg 1$ and the equations become

$$mm' = q,$$
$$q' = (m)^{1/2}, \tag{16}$$

which are the equations for a vertical plume given in eq. (5a) above.

Otherwise, however, by substituting $t \equiv (m^2-1)^{1/2} = \tan\theta$, the equations can be written

$$t' = q/(t^2+1)^{1/2},$$
$$q' = (t^2+1)^{1/4}, \tag{17a}$$

This is the final form of the equations used in this model. The initial conditions are

$$t_S = \tan\theta_S, \qquad q_S = (\lambda/(2\alpha)^{1/2}) F_0^{1/2} H_0^{-5/4} Q_S, \tag{17b}$$

where the dimensionless mass flux is obtained from (14).

4. Solutions for forced, angled plumes

Equations (17a) were integrated numerically, using various initial values of the inclination θ and setting q initially to zero. All plumes can be traced back to a virtual origin where q, the mass flux, is zero. Hereafter the subscript 0 will refer to conditions at the virtual origin, the subscript S to those at the actual source of a plume. (Note that $F_0 = F_S$ and $H_0 = H_S$ since these quantities are conserved throughout the plume.)

The trajectory of the plume centre-line can be determined from

$$x' = \cos\theta \qquad \text{and} \qquad z' = \sin\theta. \tag{18}$$

All other plume properties can be recovered from q and θ:

$$\Delta\rho = \rho g'/g = \Delta\rho_S q_S/q,$$
$$M = H_0/\cos\theta,$$
$$R = R_S(q/q_S)(\cos\theta/\cos\theta_S)^{1/2}, \tag{19}$$
$$V = V_S(q_S/q)(\cos\theta_S/\cos\theta).$$

Figure 8 shows the values of q and θ along plumes for various values of θ_0 at $q=0$. For any given real plume, q_S can be calculated from (17b), which, rearranged, gives

$$q_S = (\lambda/(2\alpha)^{1/2})(g'R/V)^{1/2}(\cos\theta_S)^{-5/4}. \tag{20}$$

The centre-lines of plumes with different angles at the virtual origin are plotted in Fig. 9. The values of plume length s measured from the virtual origin are given on both Fig. 8 and 9 to facilitate identification between them. The position on Fig. 9 is determined by the value of s and virtual origin angle, θ_0, found from Fig. 8. For example: if, for a given real plume, $q_S = 2.5$ and $\theta_S = 10°$ at the source then it can be seen (from Fig. 8) that this is equivalent to a position part way along a plume whose initial conditions were $q=0$ and $\theta = -60°$, at a distance 2.0 (measured along the plume axis) from the source. This is at

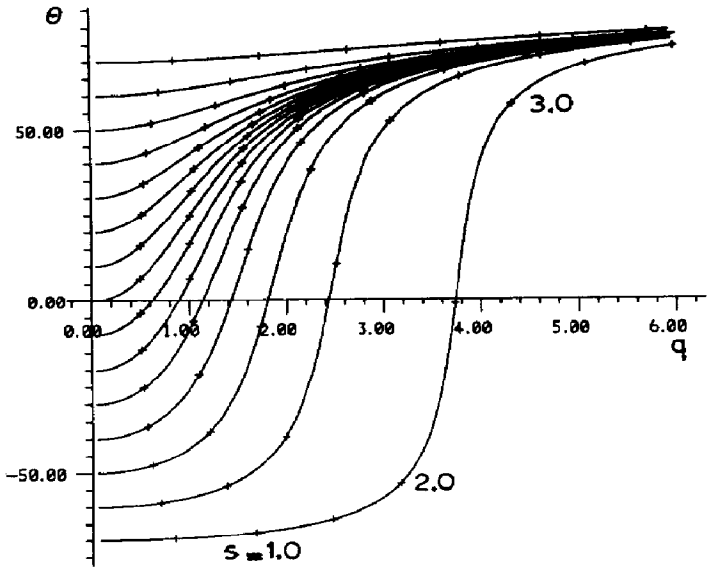

Fig. 8. Non-dimensionalised mass flux as a function of plume angle for various values of the plume angle at the virtual origin. The solutions have been marked at points corresponding to regular intervals measured along the plume centre-line to ease identification between this figure and the next.

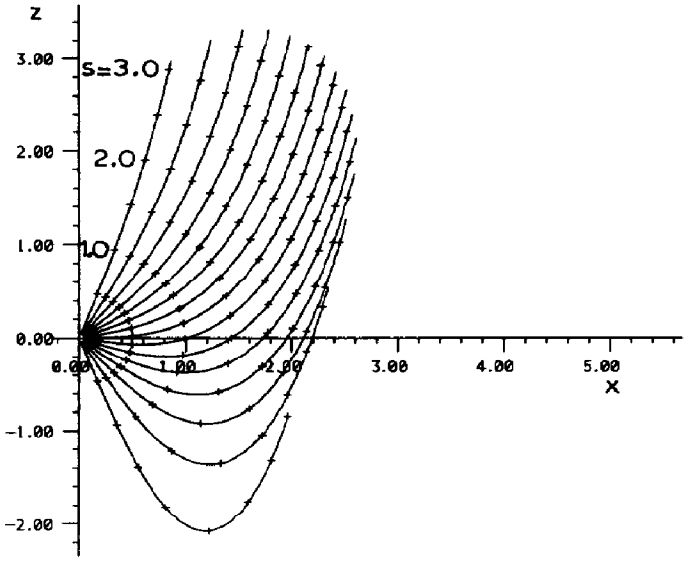

Fig. 9. Shapes of the centre-lines of angled plumes with the same range of initial angles as for Fig. 8. The marks on each solution are at regular intervals measured along the plume centre-line.

$x=1.3$, $z=-1.4$ on Fig. 9, the centre-line of the real plume is then given by following the curve through $(1.3, -1.4)$ for higher values of s. The *shape* of a plume depends only on its angle at its virtual origin, though its overall *size* varies, depending on the length scale defined in (14).

The shape of the boundaries of plumes with various values of θ_0 are shown in Fig. 10, though note the warnings given below in interpreting these figures. It is sometimes useful to know the lowest point reached by a buoyant plume which has a downward component of momentum flux at the source. This can be estimated by dimensional analysis: see, for example, Fischer et al. [11]. A length-scale can be made from the buoyancy flux and the vertical component of the momentum flux, $(M_0 \sin\theta_0)^{3/4} F_0^{-1/2}$, and it has been proposed that this length-scale multiplied by a universal constant will give the lowest point of the plume. Figure 11 shows the relationship between the lowest point, z_M, measured from the virtual origin, and the value of θ_0. Since this distance is measured from the virtual origin this figure is most useful where the actual source is close to the virtual origin, i.e. when q_S is small. Note that in Fig. 11 the lengths are non-dimensionalised with respect to the buoyancy flux and the *total* momentum flux at the virtual origin, rather than the *horizontal* momentum flux, so Fig. 11 gives the relationship between the lowest point and θ_0 for a given total momentum flux at the virtual origin. The total momentum flux at the virtual origin, proportional to M_0, is related to the (constant) horizontal momentum flux and thence the total momentum flux at the source by

$$M_0 \cos\theta_0 = H_0 = H_S = M_S \cos\theta_S. \tag{21}$$

It can be seen that the relationship between z_M and θ_0 given in Fig. 11 is a nearly linear one and it is significantly different from a curve of the form $(\sin\theta_0)^{3/4}$ given by the dimensional analysis described above. Also plotted on Fig. 11 are the results of laboratory experiments, described below. The larger error bars at larger angles to the horizontal are due to features of the flow: large eddies develop and though the boundary (of interest) of the plume is well defined at any instant its position is subject to large fluctuations.

For such plumes it is also useful to know where the plume returns to its original level (its "range") and its concentration there. In general it is necessary to evaluate the behaviour of the plume from its initial conditions using Figs. 8 and 9 and eq. (19). If q_S is small, however, the actual source is close to the virtual origin and θ_S is close to θ_0. Thus the range is (approximately) the value of x where the plume returns to $z=0$. Again, to make clear the dependence on θ_0, we will non-dimensionalise the mass flux and lengths with respect to the total momentum flux, M_0, so that

$$q_1 = (\lambda/(2\alpha)^{1/2}) M_0^{-5/4} F_0^{1/2} Q, \tag{22}$$

and the new length-scale is given by $L_1 = (\lambda\sqrt{\alpha})^{-1} M_0^{3/4} F_0^{-1/2}$.

Figure 12 shows the range, both to the nearest point on the plume at $z=0$, denoted by x_{1B}, and the distance to the centre-line at $z=0$, denoted by x_{1C}, as it depends on θ_0. Figure 13 shows $1/q_1$ at these positions, which is proportional to concentration (see eq. 19), though note that the model assumes a top-hat form of the concentration profile and this needs to be considered when evaluating the value at the near boundary, x_{1B}.

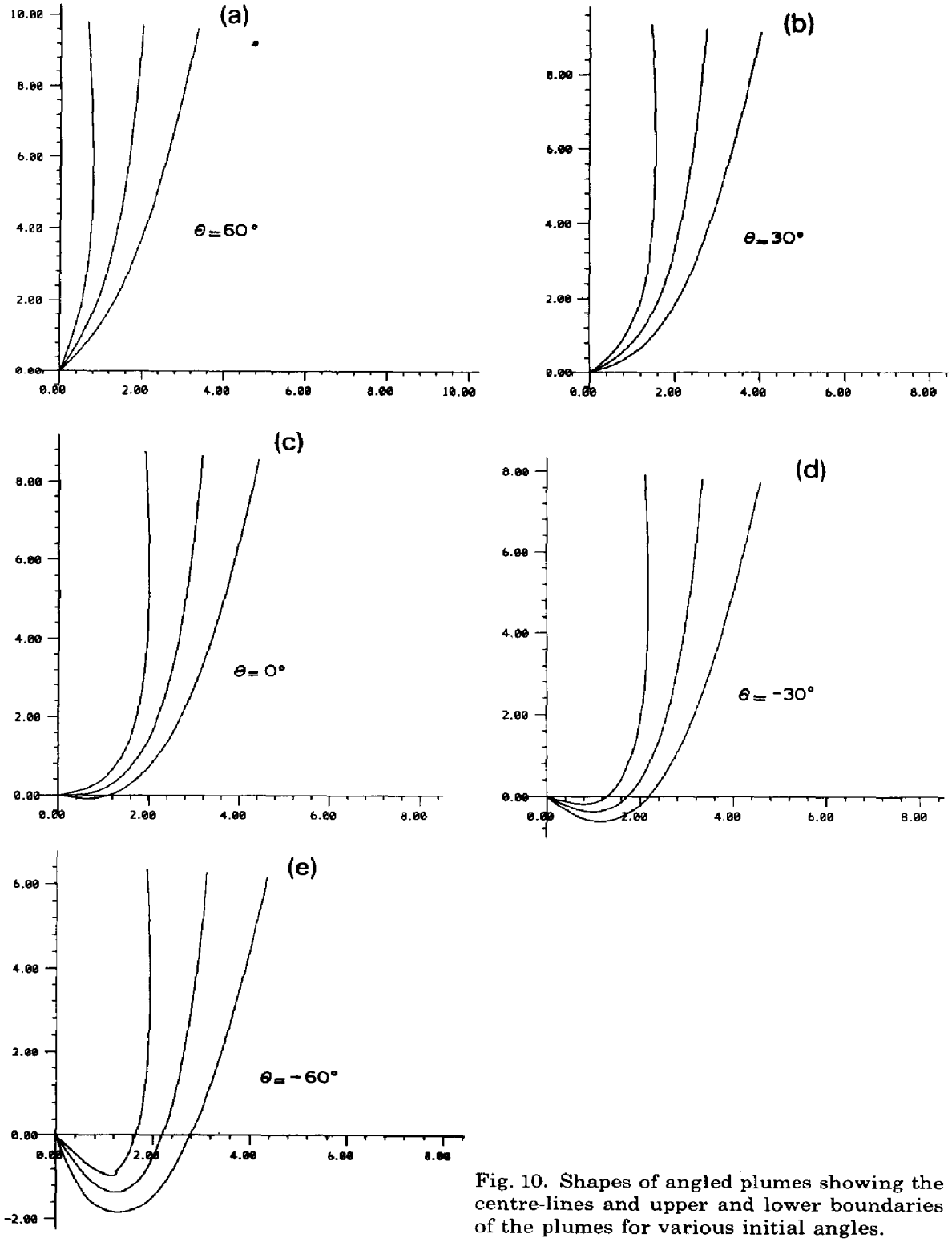

Fig. 10. Shapes of angled plumes showing the centre-lines and upper and lower boundaries of the plumes for various initial angles.

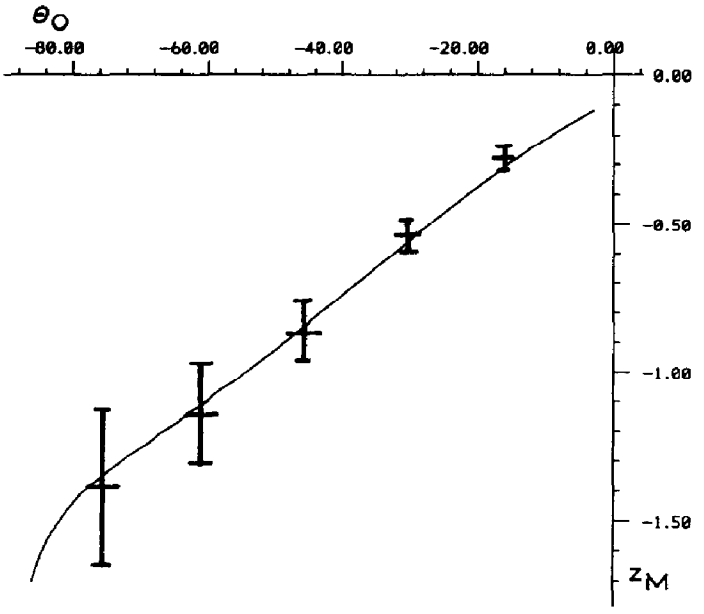

Fig. 11. Theoretical and experimental results showing the maximum depth that the lower boundary of a downward angled plume reaches. The lengths have been non-dimensionalised with respect to the total momentum flux (rather than the horizontal momentum flux) at the virtual origin. The error bars reflect the uncertainties in the maximum depth due to fluctuations of the turbulent plume.

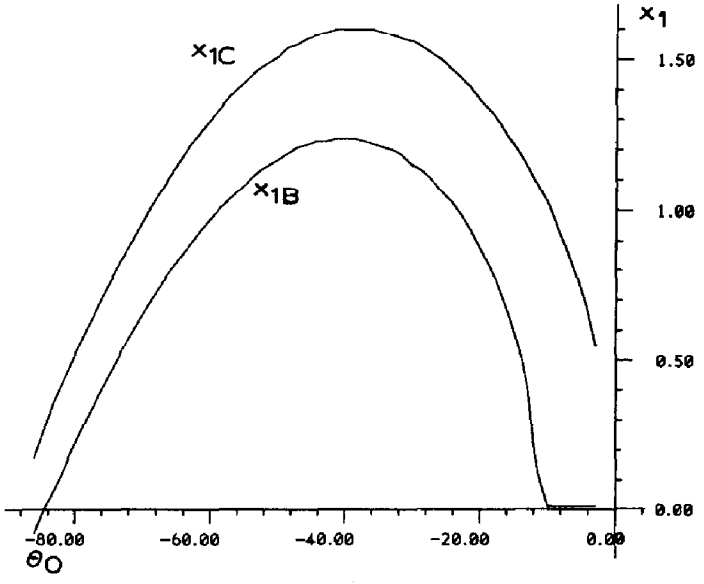

Fig. 12. The distance from the virtual origin to the point on a downward angled plume where it returns to its initial height, with x_{1B} the distance to the upper boundary, and x_{1C} the distance to the centre-line.

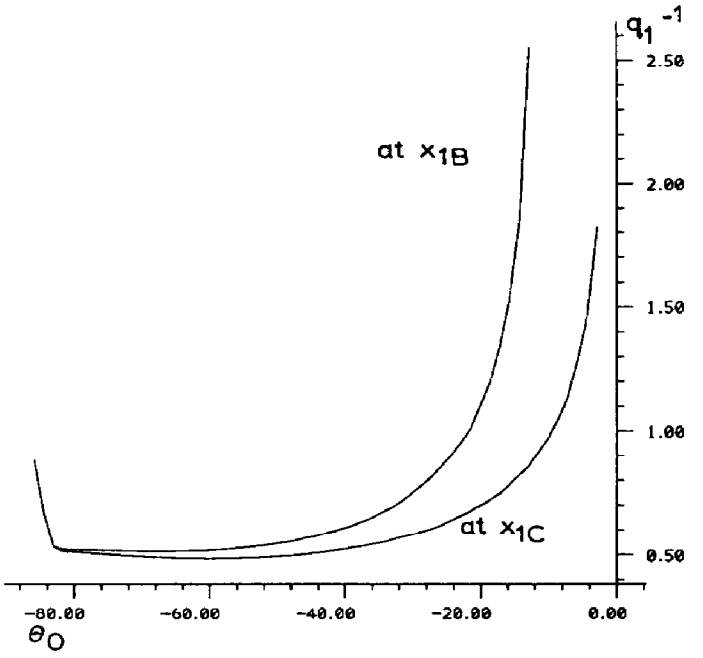

Fig. 13. The value of $1/q_1$ at the point where a downward angled plume returns to its initial height. This is a measure of the concentration at that point (see text).

5. Discussion of the theoretical results

Figure 14 shows the radius and speed of the plume as a function of position along the plume centre-line for $\theta_0 = +45°, 0°, -45°$. The results for $\theta_0 = +45°$ are similar to those for a vertical plume with, initially, a momentum jet behaviour tending to a buoyant plume shape as in Fig. 3, but with the centre-line following a curved trajectory. For $\theta_0 = 0°$ (a horizontal jet) the results are again similar but here the transition from momentum jet, with spreading angle $\tan^{-1}(2\alpha)$, to buoyant plume, with angle $\tan^{-1}(6\alpha/5)$, is somewhat sharper.

For negative θ_0, however, a different phenomenon is apparent. The vertical component of the velocity is initially negative and increases through zero as the plume turns. Thus the total plume speed is decelerated more than in the previous cases and the plume radius increases more than for a momentum jet. The plume is then accelerated (the speed of the plume has a minimum in this case as distinct from the previous cases where the plume speed decreases monotonically) and the plume radius increases more slowly than for the buoyant plume. In fact, for sufficiently steep negative angles the plume radius actually decreases. The shape is similar to the "mass source" in Fig. 3. On physical grounds the momentum jet-like behaviour can only be exhibited where the plume momentum flux has a (positive) component in the direction of

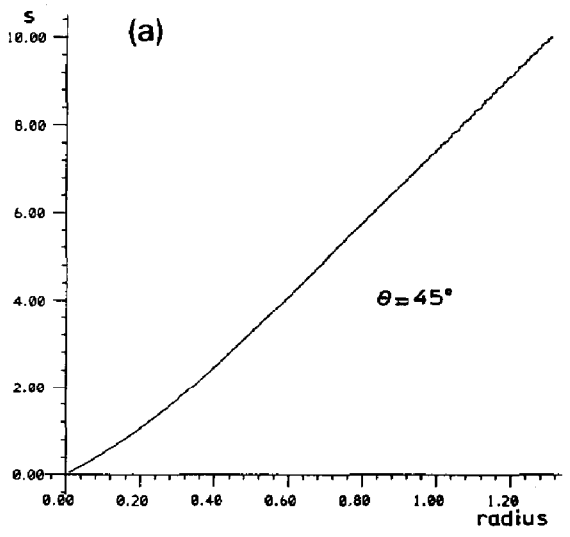
(a)
S
10.00
8.00
6.00
4.00
2.00
0.00
θ=45°
0.00 0.20 0.40 0.60 0.80 1.00 1.20
radius

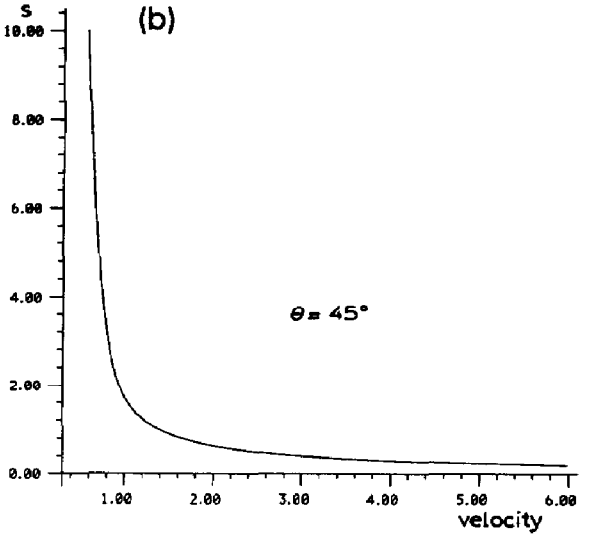
(b)
S
10.00
8.00
6.00
4.00
2.00
0.00
θ= 45°
1.00 2.00 3.00 4.00 5.00 6.00
velocity

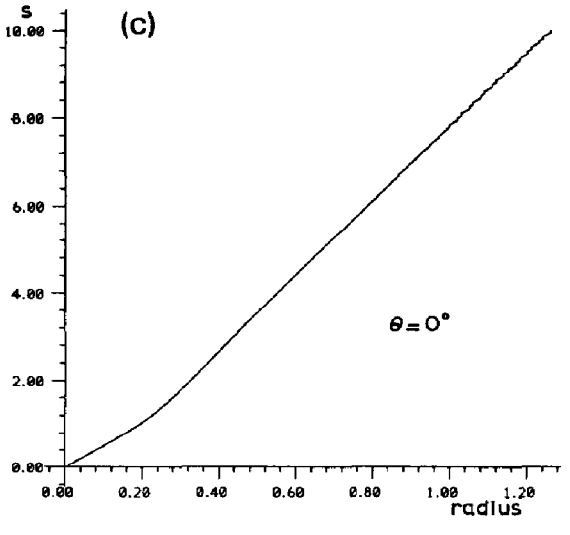
(c)
S
10.00
8.00
6.00
4.00
2.00
0.00
θ=0°
0.00 0.20 0.40 0.60 0.80 1.00 1.20
radius

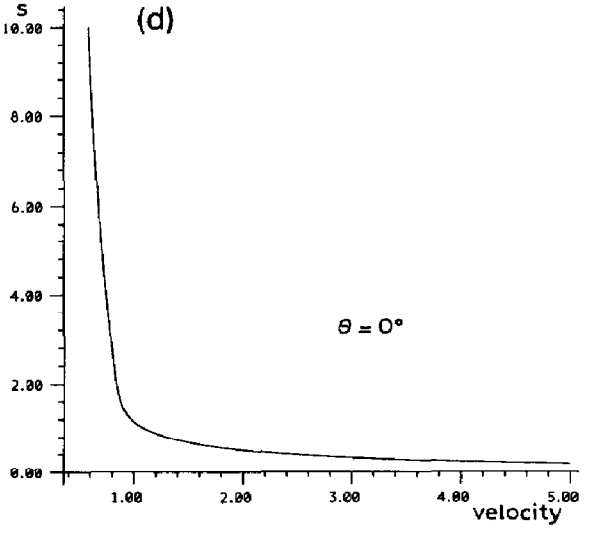
(d)
S
10.00
8.00
6.00
4.00
2.00
0.00
θ = 0°
1.00 2.00 3.00 4.00 5.00
velocity

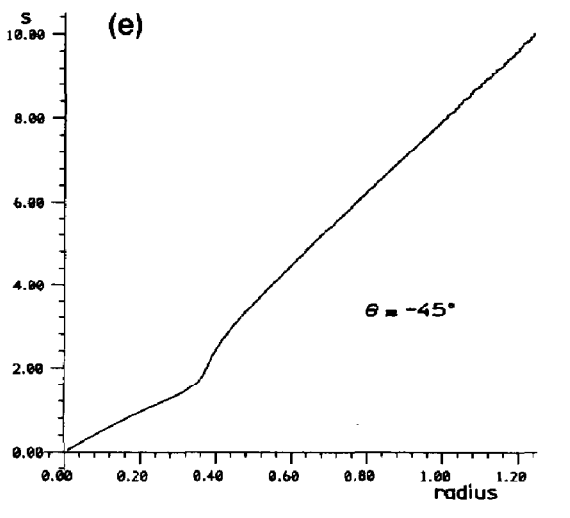
(e)
S
10.00
8.00
6.00
4.00
2.00
0.00
θ = -45°
0.00 0.20 0.40 0.60 0.80 1.00 1.20
radius

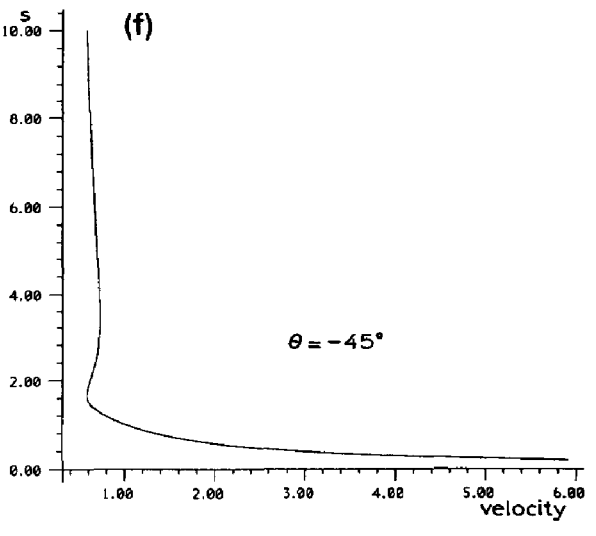
(f)
S
10.00
8.00
6.00
4.00
2.00
0.00
θ = -45°
1.00 2.00 3.00 4.00 5.00 6.00
velocity

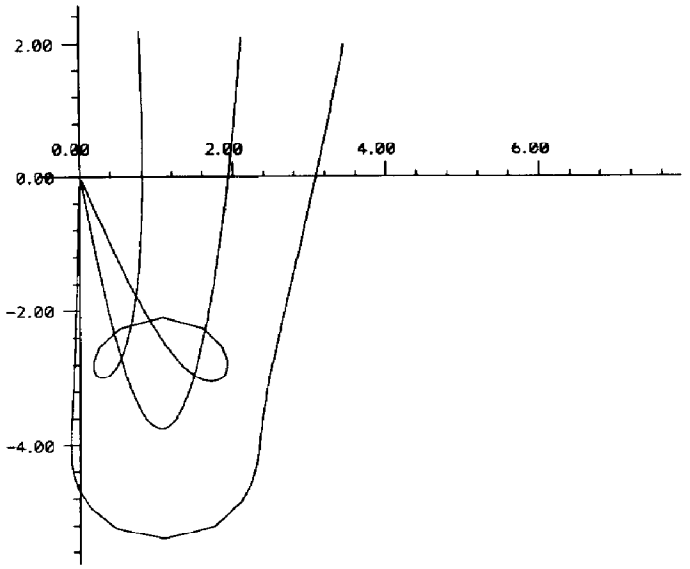

Fig. 15. Shape of plume when the initial angle is $-80°$ showing the upper and lower boundaries and the centre line. Notice that the upward flowing part of the plume overlaps the downward flowing part, thus only that part of the shape beyond the overlap will be realisable in practice.

the initial momentum flux. Thus once the plume turns and begins to rise it is (essentially) equivalent to a source of mass and buoyancy and a relatively small amount of horizontal momentum, placed at (approximately) the position where the plume turns.

Figure 15 shows the predicted plume shape for $\theta_0 = -80°$ and here the theoretical result has the plume overlapping a previous position. It is important to note that the model is invalid in such regions since it does not allow for re-entrainment of plume fluid. Thus for $\theta_0 = -80°$ the model is only valid for $s > 2.5$, where the predicted shape is not overlapped by a previous part of the flow. There is some overlap for θ_0 steeper than approximately $-75°$.

It should also be noted that the top edge of the plume is unstable in that there is light fluid below heavy fluid. Thus some fluid formerly in the plume will be detrained and rise into the region above the plume. Thus the stable, lower edges of the plume shapes shown in Fig. 10 will be sharply defined in practice, whereas the upper, unstable edges will be poorly defined. See, for comparison, the photograph of a real plume in Fig. 16, described below.

Fig. 14. The radius and along-axis speed of angled plumes as a function of distance along the plume centre-line. Notice that there is a minimum in the speed for the initially downward pointing plume.

Fig. 16. Shadowgraph of an angled plume. Here the injected fluid is denser than ambient so the buoyancy forces act downward.

6. Experiments

Forced plumes were produced by pumping salt water through a circular pipe (1.95 mm diameter) into a tank containing fresh water. Note that since the injected fluid is relatively dense, the buoyancy forces on the plume act downwards, rather than upwards as was the case for the theory above. The tank dimensions were 4 m long by 0.3 m wide and it was filled to a depth of about 0.5 m. These dimensions are large compared with typical length scales of the flow and so this configuration approximates an infinite, unstratified environment at rest. The flow rate πQ_0 was monitored with a flow meter and the buoyancy flux πF_0 and the momentum flux πM_0 were determined from

$$F_0 = g' Q_0,$$
$$M_0 = \tfrac{4}{3} Q_0^2 a^{-2}, \tag{23}$$

where a is the pipe radius.

Typical pipe nozzle Reynolds numbers were in the range 1000 to 2500 and the expression for M_0 is obtained assuming laminar Poiseuille flow in the pipe. The

pipe was set at fixed orientations θ_0 to the horizontal and the angles were measured to an accuracy of 0.5°.

The visualisation was carried out using a shadowgraph and estimates of the maximum height were made from still photographs. A conductivity probe was placed at a set of fixed positions in the flow and the salt concentration was measured to obtain information about the structure and mixing in the plume.

7. Experimental results

An example of the flow with $\theta_0 = 60°$ is shown in Fig. 16. Close to the source the plume is symmetrical but a pronounced asymmetry develops downstream. The upper side of the plume remains sharp and well defined while the lower side is diffuse and has no distinct edge even in an instantaneous picture as shown in the shadowgraph. This asymmetry results from the opposite effects of the buoyancy force on the two sides of the plume. On the upper side, buoyancy forces create a stabilizing stratification which tends to inhibit entrainment of the environmental fluid. On the lower side the buoyancy forces produce a convectively unstable configuration and there is enhanced mixing between the plume and the environment. *Detrainment* of plume fluid is observed on the lower side, a feature which is not observed in vertical plumes.

Measurements of the structure of the plume were made for an initial inclination of 45° using a conductivity probe. Figure 17 shows the density contours in a plane normal to the plume axis positioned at the point of maximum plume height. The asymmetry between the upper and lower parts of the plume can be clearly seen. Near the top of the plume there is a strong, stable density gradient. Below the plume axis the dense fluid is mixing much more vigorously with the surrounding fluid as a result of the gravitational instability. Density profiles in a vertical plane containing the plume axis are shown in Fig. 18a.

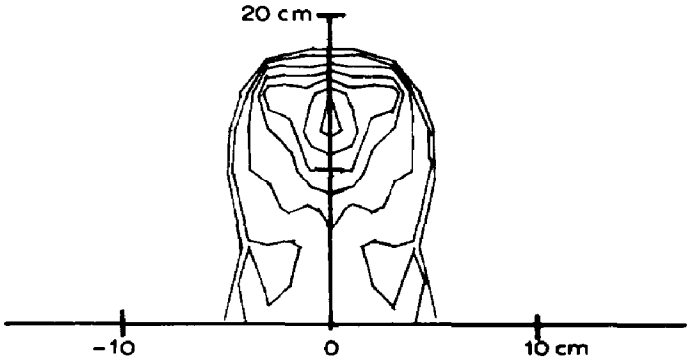

Fig. 17. Experimentally observed, time-averaged, measurements of concentration in a plane perpendicular to the plume axis, at the highest point on the plume. The injected fluid was denser than ambient, and injected at an angle of 45° above the horizontal. Notice the detrainment of fluid from the lower, unstable edge of the plume.

The asymmetry between the upper and lower parts of the plume is seen to increase with distance downstream. The estimated plume axis (line of maximum density excess) is shown in Fig. 18b, as is the theoretically predicted plume axis. The discrepancy is due partly to experimental errors, in particular in measuring the source radius accurately and in measuring the relatively weak concentrations far from the source, and partly due to using a fixed value of α that is certainly too large for the jet part of the flow, and may be too large for the mass-source part of the flow. The mean value of the density difference on the plume centre-line is plotted on Fig. 19, as is the theoretical prediction. Note that the observed density difference is generally larger than the prediction, suggesting less entrainment than predicted (smaller α), which would lead to greater vertical acceleration.

The maximum height to which the upper plume boundary rose, z_M, was measured from photographs, and non-dimensionalised with respect to the length-scale L_1 (see eq. 22). These results are shown on Fig. 11, where each point represents the average over several experiments with different values of the flow rate. The comparison with the theoretical results was discussed in Section 4. Some experiments were performed with the tube set vertically, so

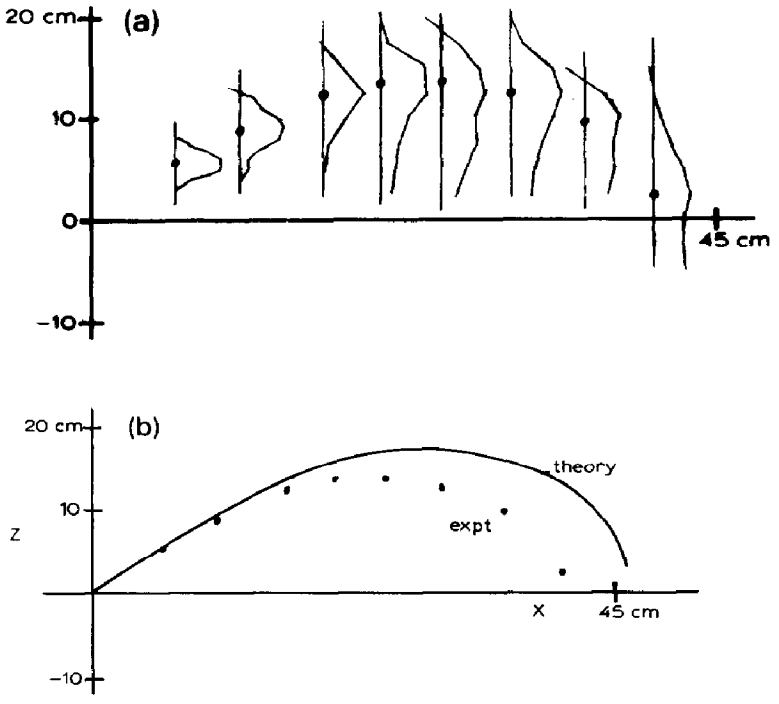

Fig. 18. (a) Vertical, time-averaged concentration profiles measured at various points along the plume centre-line. The injected fluid is denser than the surrounding fluid and was injected at 45°. (b) Position of the plume centre-line estimated from the experimental results shown in (a) (peak in density profile), with the expected centre-line for comparison. (Non-dimensional scales.)

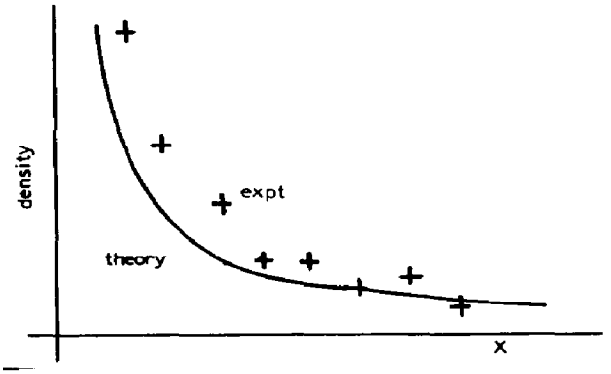

Fig. 19. Density difference between the plume fluid and the ambient fluid from the experiment shown in Figs. 16 to 18 (time-averaged on the plume centre-line), with the theoretical result shown for comparison. (Non-dimensional scales.)

that the rising part of the plume entrains fluid that is falling back down. This height cannot be predicted by the theory above, since it assumes that only ambient fluid is entrained. These experiments gave a value of the maximum height of $z_M(90°) = 0.83 \pm 0.02$, in agreement with the value found by Turner [12]. Note that this is much smaller than the value of approximately 1.8 predicted by the model, which does not include re-entrainment of the plume fluid. Thus the re-entrainment of plume fluid has a substantial effect on the plume.

8. Conclusions

The equations for a forced, angled plume can be simplified by non-dimensionalisation with respect to two conserved quantities, namely the buoyancy flux and the horizontal component of the momentum flux. All such plumes can be traced back to a virtual origin, and the *shape* of the plume depends only on the angle of the plume to the horizontal at this virtual origin. Vertical plumes can be included in this scheme, with virtual origin angle $\pm 90°$. All angled plume shapes can be grouped into three categories, first introduced to describe vertical plumes:

(i) If the momentum flux at the virtual origin is zero then no angle can be defined and we have the special case of the vertical, straight-sided, *pure plume*, half-angle $\tan^{-1}(6\alpha/5)$.

(ii) If the momentum flux at the virtual origin is upward (or horizontal) then the plume spreads initially at a half-angle of $\tan^{-1}(2\alpha)$. We have referred to this category as the *buoyant jet*. The plume centre-line curves towards the vertical and the spreading angle tends (downward) to that of the pure plume. The change from the jet spreading angle to the plume angle occurs more sharply for plumes directed further from the vertical.

(iii) If the momentum flux at the virtual origin is downward then the initial spread is as for a jet. In this case the fluid is decelerated by the buoyancy force and the spreading angle increases. As the plume centre-line curves

upward the fluid is accelerated and the spreading angle decreases, for plumes with virtual origin angle less than approximately $-60°$ the radius actually decreases. As the plume centre-line curves upward the spreading angle tends (upward) to that of the pure plume. This category we have referred to as the *mass-source*. In this case the mean along-plume velocity has a minimum and a maximum (see Fig. 14), whereas the velocity decreases monotonically for cases (i) and (ii). Note also that part of the solution near the virtual origin will be unphysical for sufficiently steep values of θ_0, due to the model not allowing for re-entrainment of plume fluid. In particular, for $\theta_0 = -90°$ the solution is unphysical until the flow is upward.

The overall *size* depends on the length scale L_A defined above. For the vertical plumes it is, however, necessary to trace the solution back to the virtual origin to find a useful scale for the momentum flux, which can be used to define a length-scale, L_V. Because of this last feature we regard vertical plumes as a very special case of the generality of angled plumes. This is in contrast to the usual approach which is to consider plumes with a horizontal component of momentum flux as merely a minor departure from the vertical case, as is, for example, implicit in the dimensional analysis approach to predicting maximum depth of a downward angled buoyant plume, or explicit in the approach used by Germeles [4].

The virtual origin angle, and thus the shape of the plume, can be determined from the source angle and the non-dimensionalised source mass flux. While the variations of the velocities and densities from the mean and the details of the eddies and entrainment is beyond the scope of this approach, we have shown that the theory predicts some of the mean properties and the basic shape of such plumes reasonably accurately. In fact the entrainment assumption describes the flow surprisingly accurately, given that the observed velocity and density distributions are neither symmetric nor self-similar. We conclude that the average entrainment into the plume is described adequately by an average entrainment velocity proportional to the mean velocity in the plume.

In this model we have kept α constant, though there is evidence that the nature of the entrainment, and thus the value of α, varies for different types of plume flow (see, for example, Turner [12]). Altering the value of α alters the local length-scale and the spreading angle of the plume, and the experimental evidence is that this reduces the difference in spreading angle between jet and plume flows predicted by theories such as the one given here. One may regard different spreading angles predicted by our theory as pointing out changes in the nature of the flow, and thus the entrainment, at different points on the plume. It would be possible to recalculate the results with α allowed to vary according to the local nature of the flow. It is important to note that this would not affect the result that the plume shape is entirely determined by the virtual origin angle, since different plumes with the same virtual origin angle would have changes, e.g. from jet to plume behaviour, at equivalent points on the plume.

This model does not allow for stratification in the ambient fluid. In many cases the stratification will not be important until the plume is rising almost vertically, where previous models (e.g. [2, 3]) can be used. Stratification will not be important in the neighbourhood of the source provided that the density changes in the ambient fluid over the length scale of the plume are small compared with the density difference between the plume and the ambient fluid. This criterion requires

$$N \ll F_0/H_0, \tag{24}$$

where the ambient stratification has buoyancy frequency $N=(-g(\partial\rho/\partial z)/\rho)^{1/2}$.

When stratification is important this can be taken into account by modifying equation (11) (the buoyancy flux is no longer constant) so that the right hand side of the density difference equation becomes N^2VR^2. However, this is not entirely satisfactory since under such strong stratification the plume cross-section becomes elliptical, with greater spread in the horizontal direction and reduced spread in the vertical direction because vertical motions are impeded by the stratification. The reader is recommended to see Hofer and Hutter [6] for a more detailed analysis.

Acknowledgements

G.F.L-S was supported by a Research Scholarship from British Gas plc when conducting this work, and M.H. by a grant from the Wolfson Foundation.

References

1 B.R. Morton, G.I. Taylor and J.S. Turner, Turbulent gravitational convection from maintained and instantaneous sources, Proc. R. Soc., 234 (1956) 1–23.
2 B.R. Morton, Forced plumes, J. Fluid Mech., 5 (1959) 151–163.
3 B.R. Morton, The ascent of turbulent, forced plumes in a calm atmosphere, Int. J. Air Water Pollut., 1 (1959) 184–197.
4 A.E. Germeles, Forced plumes and mixing of liquids in tanks, J. Fluid Mech., 71 (1975) 601–623.
5 M. Schatzmann, The integral equations for round buoyant jets in stratified flows, J. Appl. Math. Phys. (ZAMP), 29 (1978) 608–620.
6 K. Hofer and K. Hutter, Turbulent jet diffusion in stratified, quiescent ambients. Part 1: Theory. J. Non-Equil. Thermodyn., 6 (1981) 31–48.
7 G.I. Taylor, Dynamics of a mass of hot gas rising in air, U.S. Atomic Energy Commission MDDC 919. LADC 276, 1945.
8 E. List, Turbulent jets and plumes, Annu. Rev. Fluid Mech., 14 (1982) 189–212.
9 J.S. Turner, Buoyancy effects in fluids, Cambridge University Press, Cambridge, 1973.
10 H. Rouse, C.S. Yih and H.W. Humphreys, Gravitational convection from a boundary source, Tellus, 4 (1952) 201–210.
11 H.B. Fisher, E.J. List, R.C.Y. Koh, J. Imberger and N.H. Brooks, Mixing in Inland and Coastal Waters, Academic Press, New York, 1979.
12 J.S. Turner, Jets and plumes with negative or reversing buoyancy, J. Fluid Mech., 26 (1966) 779–792.